

## Relaxation of Electron Carriers in the Density of States of Nanocrystalline TiO<sub>2</sub>

Luca Bertoluzzi,<sup>†</sup> Isaac Herraiz-Cardona,<sup>†</sup> Ronen Gottesman,<sup>‡</sup> Arie Zaban,<sup>‡</sup> and Juan Bisquert<sup>\*,†</sup>

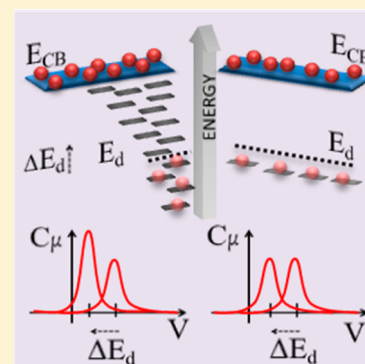
<sup>†</sup>Photovoltaics and Optoelectronic Devices Group, Departament de Física, Universitat Jaume I, 12071 Castelló, Spain

<sup>‡</sup>Institute for Nanotechnology & Advanced Materials, Department of Chemistry, Bar Ilan University, Ramat Gan 52900, Israel

### Supporting Information

**ABSTRACT:** Band gap localized states and surface states play a dominant role in the application of nanocrystalline metal oxides to photovoltaics and solar fuel production. Electrons injected in nanocrystalline TiO<sub>2</sub> by voltage or photogeneration are mainly located in band gap states. Therefore, charging a nanoparticulate semiconductor network allows one to recover the density of states (DOS) in the energy axis. However, shallow traps remain in equilibrium with the conduction band electrons, while deep traps do not. We show that the characteristic peak of the apparent DOS mixes an exponential DOS and a monoenergetic surface state. A model that incorporates the trap's kinetics proves to be very efficient to assess the important parameters that determine both contributions via variation of charging rate. Contrary to the common theory, we demonstrate that the peculiar capacitance peak of nanocrystalline TiO<sub>2</sub> can be mainly attributed, in some cases, to deep traps in the exponential distribution.

**SECTION:** Physical Processes in Nanomaterials and Nanostructures



Nanocrystalline TiO<sub>2</sub> has been widely studied for application in photovoltaics,<sup>1,2</sup> solar photocatalysis,<sup>3</sup> solar fuel production,<sup>4</sup> and lithium batteries.<sup>5</sup> The photovoltaic materials normally consist of colloidal particles or crystallites, sintered on top of a conducting glass to form a rigid framework with high internal surface area. Early work on nanocrystalline TiO<sub>2</sub> showed that electronic trap filling has enormous influence on the long-time dynamics of the dye-sensitized solar cells,<sup>6</sup> and thereafter, electron-transport measurements have been widely interpreted in terms of the multiple trapping model.<sup>7,8</sup> However, the nature and kinetic behavior of localized electronic states in nanocrystalline anatase has not been determined yet. In this Letter, we show that a combination of voltage- and time-dependent charging–discharging scans reveals the dominant contributions of the localized states in the band gap of the metal oxide semiconductor.

The density of states (DOS) of a semiconductor in the energy axis can be established by capacitance techniques applied to a semiconductor/electrolyte junction<sup>9,10</sup> that provide the chemical capacitance,<sup>11</sup> also termed a thermodynamic DOS.<sup>12</sup> The capacitive behavior of random nanoparticulate TiO<sub>2</sub> films has been widely studied,<sup>13–16</sup> and the measurements show two distinct components of the DOS, as shown in Figure 1a and b. The first feature at negative potentials is an exponential band tail that enters the gap of the semiconductor from the conduction band or mobility edge at energy  $E_c$  with effective DOS  $N_c$ , toward the center of the gap,  $g(E_t) = N_t / (k_B T_0) \exp[(E_t - E_c) / k_B T_0]$  (note that the voltage has an opposite sign with respect to the electron energy). Here,  $k_B$  is the Boltzmann constant,  $N_t$  is the total density of localized

states, and  $T_0$  is a parameter with temperature units that determines the depth of the distribution. This type of distribution is a common feature of many disordered bulk semiconductors.<sup>17,18</sup> In the case of nanosized TiO<sub>2</sub> particles, a quantum mechanical density functional theory (DFT) calculation indicates that the DOS originates from undercoordinated four-fold-coordinated surface Ti atoms mainly lying at the (100) edges found at the intersections between (101) surfaces.<sup>19</sup> Uncoordinated Ti surface ions are often identified as the origin of the second capacitive feature found at more positive potentials, which is a peak situated 0.3–0.5 eV below  $E_c$ .<sup>20–23</sup> Oxygen vacancies and/or Ti interstitials have been identified as a possible cause of these surface states.<sup>24–26</sup> The latter have also been obtained by first-principles quantum calculations when the TiO<sub>2</sub> cluster is coupled with a continuum solvation model.<sup>27</sup> These states should be especially abundant at corner positions of anatase nanoparticles, and a DFT calculation indicates that electronic states at these low-coordinated Ti sites become more localized with increased nanoparticle size.<sup>28</sup>

In small perturbation techniques such as impedance spectroscopy (IS), both capacitive features discussed above give distinct contributions in the capacitance voltage plots. For techniques using larger perturbations, such as voltammetric techniques, it may seem to be the case too, as suggested by the capacitance measurements of Figure 1a and b obtained by cyclic

**Received:** December 21, 2013

**Accepted:** January 27, 2014

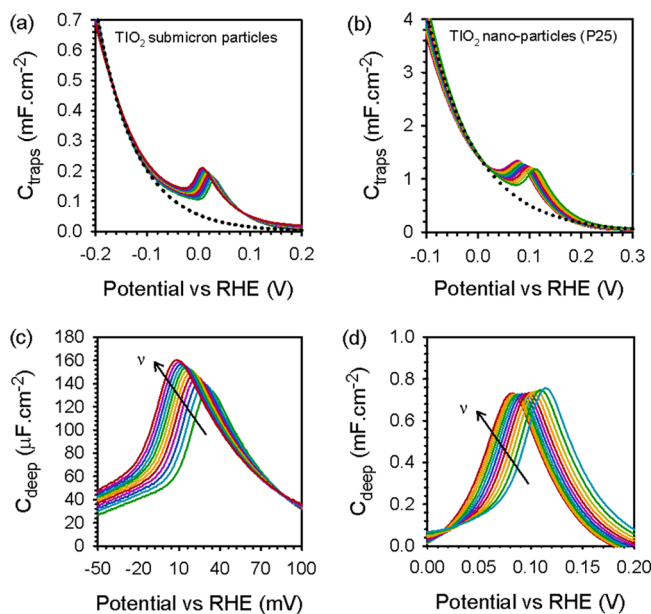


**Figure 1.** Evolution of the trap's chemical capacitance with voltage, obtained from cyclic voltammeteries at scan rates ranging from 340 mV/s to 780 mV/s for the TiO<sub>2</sub> submicrometer particles (a) and nanoparticles (P25) (b). The black dotted line corresponds to the shallow trap capacitance. Evolution of the deep trap chemical capacitance with varying scan rate for the TiO<sub>2</sub> submicrometer particle (c) and P25 samples (d).

voltammetry. However, below, we show that the peak observed at a more positive potential contains not only the component of the monoenergetic states but also components from the exponential DOS. This is revealed by the fact that the amplitude of the peak depends on the scan rate, as depicted by Figure 1c. In order to distinguish between both features of the TiO<sub>2</sub> DOS previously pointed out, we develop in the following a method to extract the energetic and kinetic parameters of the traps from capacitance measurements at various scan rates.

We describe the kinetics of localized states in terms of the exchange of electrons with the extended states of the conduction band edge. The conservation equation models such exchanges for a localized state at energy  $E_t$  with fractional occupancy  $f$  as follows

$$\frac{\partial f}{\partial t} = \beta_n n_c [1 - f] - \varepsilon_n f \quad (1)$$

Here,  $n_c$  is the number of electrons in the transport state (conduction band edge),  $\beta_n$  is the time constant per unit volume for electron capture, usually given in terms of the thermal velocity of the electrons,  $v_{th}$ , and the capture cross section,  $\sigma_{n\omega}$  ( $\beta_n = v_{th}\sigma_{n\omega}$ ), and  $\varepsilon_n$  is the rate constant for electron release, obtained by detailed balance at temperature  $T$ ,  $\varepsilon_n(E_t) = \beta_n N_c e^{(E_t - E_c)/k_B T}$ .

At this stage, it is useful to stress upon the main difference between the behaviors of the trapped carriers when performing a small or large perturbation measurement. For a small perturbation, eq 1 becomes

$$\frac{\partial \hat{f}}{\partial t} = -(\beta_n \bar{n}_c + \varepsilon_n) \hat{f} \quad (2)$$

In the above equation,  $\hat{x}$  and  $\bar{x}$ , respectively, refer to a small perturbation and a steady-state quantity. Equations 1 and 2 are

equivalent to stating that a localized state at energy  $E_t$  is filled by electrons from the conduction band at a rate  $\tau_{tr}$  and those released at a rate  $\tau_{dtr}$  where  $\tau_{tr} = (\beta_n \bar{n}_c)^{-1}$  is the response time for trapping, defined by

$$\begin{aligned} \tau_{tr}^{-1}(t) &= \beta_n N_c e^{(E_{Fn}(t) - E_c)/k_B T} \\ &= \tau_0^{-1} e^{(E_{Fn}(t) - E_{F0})/k_B T} \end{aligned} \quad (3)$$

Here,  $E_{Fn}$  is the electron Fermi level with value  $E_{F0}$  at equilibrium, and  $\tau_0$  is the trapping lifetime of free electrons at equilibrium.<sup>29</sup>  $\tau_{dtr}$  is the response time for release

$$\begin{aligned} \tau_{dtr}^{-1} &= \varepsilon_n \\ &= \tau_0^{-1} e^{(E_t - E_{F0})/k_B T} \end{aligned} \quad (4)$$

Thus, we can define a characteristic decay time,  $\tau_{dc}$ , of the fractional occupancy  $\hat{f}$  such that

$$\tau_{dc}^{-1} = \tau_{tr}^{-1} + \tau_{dtr}^{-1} \quad (5)$$

$\tau_{dc}$  can be also written using eqs 3–5 as

$$\tau_{dc} = \frac{1}{\beta_n N_c e^{-E_c/k_B T} e^{E_t/k_B T} + e^{E_{Fn}/k_B T}} \quad (6)$$

From eq 6, it is clear that when traps are thermalized to a common Fermi level, the decay, for states in which  $E_{Fn} < E_t$  is controlled by  $\tau_{dtr}$ , so that the traps are unoccupied and available for electron capture. On the contrary, for traps such that  $E_t < E_{Fn}$ , the decay is controlled by the release time.

For larger perturbation techniques such as voltammetric measurements, the occupancy of band gap states may depart substantially from the thermal equilibrium value. Indeed, because the release time  $\tau_{dtr}$  increases exponentially with the depth of the state in the band gap, not all of the states below the Fermi level can equilibrate with the substrate in a charge–discharge measurement with fast voltage sweep. Consequently, a large perturbation technique is a way to probe the internal kinetics of electrons in a semiconductor electrode. For this kind of measurements, it is therefore necessary to distinguish between the dynamics of two types of traps, as indicated in Figure 2, shallow traps that remain at equilibrium with the substrate (via transport of free carriers in the conduction band) from deep traps that do not (due to kinetic limitations). The

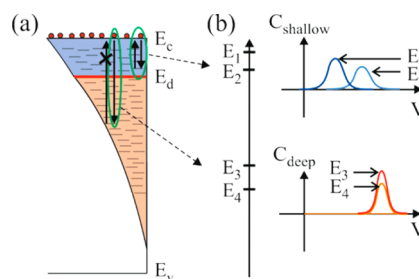


**Figure 2.** (a) Scheme of TiO<sub>2</sub> energetics, including the edges of the conduction  $E_c$  and valence  $E_v$  bands and the characteristic exponential DOS of band gap localized states. The trapping/detrapping dynamics are also shown by the down/up orientated arrows. The demarcation level  $E_d$  indicates the separation between the dynamics of the shallow and deep states. (b) Typical capacitance–voltage patterns of two shallow localized states at the energies  $E_1$  and  $E_2$  ( $E_1 > E_2$ ) and two deep localized states at the energies  $E_3$  and  $E_4$  ( $E_3 > E_4$ ) above and below  $E_d$ , respectively.

energetic level that separates both kinds of traps will be herein referred as the demarcation energy level  $E_d$ , which will be calculated later on. Note that the faster the scan rate  $\nu$  of the charge–discharge measurement, the higher the number of traps that are not at equilibrium with the substrate. As a consequence, the demarcation level must shift up with scan rate. Note that this demarcation level is different from, though analogous to, the one introduced by Bisquert et al.<sup>30</sup> in the presence of recombination at the interface semiconductor/electrolyte or by Orenstein and Kastner<sup>31</sup> in the case of carrier relaxation into deep band gap states after photoexcitation by a laser pulse.

As discussed in a previous work<sup>32</sup> and shown in Figure 2b, the apparent chemical capacitance associated with deep traps reaches a peak when charging the material and remains zero when subsequently discharging it. Besides, in the dynamic regime, deep traps, unlike shallow traps, exclusively depend on the trapping rate and are therefore independent of the energy level of the localized states. As a consequence, the capacitance of any deep trap reaches a peak at the same applied voltage, independently of the energy of those traps (Figure 2b). Thus, it is impossible to distinguish between the deep traps of the exponential DOS (first capacitive feature) and the mono-energetic level of deep traps (second capacitive feature) from a single capacitance measurement. However, the capacitance peak must depend on the number of deep traps and thus on the scan rate. By increasing the scan rate of the charging measurement, it is therefore possible to vary the capacitance peak and the voltage at which the capacitance reaches this peak.

This behavior was evidenced through charging–discharging measurements by cyclic voltammetry with submicrometer particles and nanoparticles (P25) on FTO substrate that we synthesized following the method given in ref 33. More information can be found in the Supporting Information (SI) concerning the TiO<sub>2</sub> film preparation method. The nanoparticle sizes ranged between 250 and 350 nm for the submicrometer particles and were of the order of 20 nm for the nanoparticles. The submicrometer particles present the advantage to have a well-defined crystalline morphology and geometrical structure, as shown by Figure 3. They hence constitute an ideal system for our investigation, even though these particles might present some internal field distribution that we neglect here. The total thickness  $L$  of the active layer was estimated (by HRSEM examination of the sample cross section) to be 10  $\mu\text{m}$  for the submicrometer particle electrode and 14  $\mu\text{m}$  for the nanoparticle one (see the SI for the P25 HRSEM cross section).

The chemical capacitance was extracted from charge–discharge experiments by application of a linear potential. Measurements were performed using a FRA coupled PGSTAT-302 Autolab potentiostat controlled with Nova 1.10 software. A conventional single-compartment three-electrode cell consisting of a 1 cm<sup>2</sup> geometric area FTO/TiO<sub>2</sub> working electrode, a Pt net counter electrode, and a Ag/AgCl (3 M KCl electrolyte) reference electrode (−0.27 V versus RHE) was employed. In order to minimize the effect of the FTO substrate, the exposed FTO surface, not covered by TiO<sub>2</sub> particles, was passivated by a nonconductive resin. The electrolyte was an aqueous solution of 0.1 M HCl. Charge–discharge measurements were recorded from 1.1 to −0.4 V versus RHE at different scan rates ranging from 340 to 780 mV s<sup>−1</sup>. Indeed, at lower scan rates (inferior to the 340 mV s<sup>−1</sup> step), the capacitance amplitude for the submicrometer particles was too small to reliably measure it,

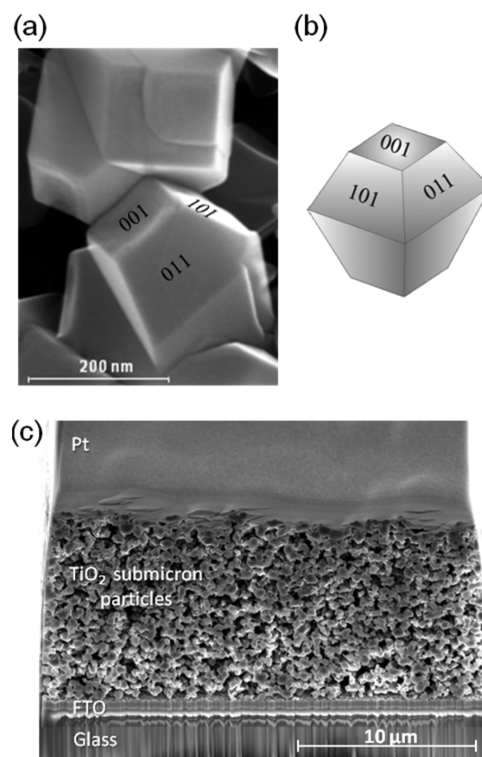


**Figure 3.** (a) HRSEM top-view image of a low surface area submicrometer anatase TiO<sub>2</sub> electrode. (b) Scheme of an anatase submicrometer particle. (c) HRSEM cross section of the same electrode.

while at higher scan rates (superior to 780 mV s<sup>−1</sup>), the scan sweep was too fast to let the time to the trap states be filled, and the trap capacitance decreased. Prior to each scan, the working electrode was held at 1.1 V versus RHE for 1 min in order to set up the same electrode initial state. The stability of the working electrode was assessed by sequentially repeating the experiments three times. The results of the capacitance measurements are summarized in Figure 1. The details on the method of extraction of the capacitances of Figure 1 are given in the SI.

In order to assess the density of localized states and the kinetics of the system from the experimental data of Figure 1c and d, we calculated the capacitance for both types of capacitive features. It should be noted that for deep traps, the quasi-static approximation, used for techniques such as IS, is no more valid, and a nonequilibrium approach must be applied. We explain our approach as follows. During the charging experiment, the probability  $f$  of any deep trap to be occupied by an electron from the conduction band at the metal/substrate contact obeys eq 1. The voltage decreases linearly with time and displaces the electron Fermi level as  $V(t) = -(E_{Fn}(t) - E_{F0})/q = V_0 - \nu t$ , where  $V_0$  is the initial potential (here,  $V_0 = 1.1$  V). Assuming that the electron cannot be detrapped to the conduction band, we have  $\tau_{\text{dtr}}^{-1} \ll df/dt$  [equivalent to writing  $\tau_{\text{dtr}} \gg \tau_\nu = k_B T / (q\nu)$ ]<sup>32</sup>, which leads to

$$\frac{df}{dt} = \tau_{\text{tr}}^{-1}(t)(1 - f(t)) \quad (7)$$

The demarcation level can be estimated when  $\tau_{\text{dtr}} = \tau_\nu$ , and we get

$$E_d = k_B T \ln\left(\frac{\tau_0}{\tau_\nu}\right) + E_{F0}$$

$$= k_B T \ln\left(\frac{\nu}{\nu_0}\right) + E_{F0} \quad (8)$$

with  $\nu_0 = k_B T / (q\tau_0)$ . The occupation probability of deep localized states at any time can be obtained by analytically solving eq 7, assuming that traps are initially empty [ $f(t=0) = 0$ ]. Hence,  $f(t) = 1 - e^{(\tau_\nu/\tau_0(0) - \tau_\nu/\tau_0(t))}$ . It is now possible to assess the voltage of the capacitance peak by solving the equation  $d^2f/dt^2 = 0$ . Assuming that  $\tau_{tr}(t) \ll \tau_{tr}(0)$  at the peak voltage, it follows that  $e^{-qV_{peak}/k_B T} = \nu/\nu_0$ , where  $V_{peak}$  is the voltage corresponding to the deep trap capacitance peak. The total chemical capacitance for both the deep traps of the exponential DOS and the monoenergetic level of deep traps ( $N_t$  traps per unit volume) can consequently be recovered, assuming that  $E_d \gg E_\nu$

$$C_{deep}^{peak} = -qL \left[ \int_{E_\nu}^{E_d} \frac{df}{dV} \Big|_{V_{peak}} g(E_t) dE_t + N_t \frac{df}{dV} \Big|_{V_{peak}} \right]$$

$$= \frac{1}{e} \frac{q^2 L}{k_B T} \left[ N_{L0} \left( \frac{\nu}{\nu_0} \right)^\alpha + N_t \right] \quad (9)$$

where  $\alpha = T/T_0$ ,  $N_{L0} = N_L e^{\alpha(E_{F0} - E_c)/k_B T}$  and  $e = \exp(1)$ .

Equation 9 clearly displays both capacitive contributions, the capacitance from the deep traps of the exponential DOS that increases with scan rate (first term on the right-hand side of eq 9) and the capacitance associated with the monoenergetic level of states that is independent of scan rate (second term on the right-hand side of eq 9).

From Figure 1c and d, it is clear that the submicrometer particle electrode displays both capacitive contributions, while the P25 electrode is featured by a scan-rate-independent capacitive peak. This does not necessarily mean that for the P25 particles the exponential band tail of traps does not penetrate deep enough in the band gap (i.e.,  $\alpha$  too large). Instead, this absence of contribution from the deep traps of the exponential DOS can be due to fast kinetics of trapping/detrapping. This issue is discussed further below in this Letter and in the SI. From now on, we will focus only on the case of interest, which is the submicrometer particle electrode where both contributions can be directly observed. For the latter case, the experimental data of Figure 4 (red dots), extracted from Figure 1c (see the SI for more details) were fitted to eq 9, as shown by the blue solid lines of Figure 4, which allowed us to estimate the values of the densities of localized states as well as the depth of the exponential distribution and the trapping kinetics. The resulting parameters are summarized in Table 1.

From Table 1, it is now clear that  $N_t \ll N_L$ . Contrary to the common belief, the peculiar capacitive behavior of TiO<sub>2</sub> cannot necessarily be attributed to a monoenergetic level of traps. In fact, for the submicrometer particle electrode, the monoenergetic states at the anatase surface are in negligible quantity due to the crystalline features of our samples and the use of an acidic electrolyte. However, the inherent undercoordinated four-fold-coordinated surface Ti atoms are still present, as demonstrated by ref 19. In this configuration, electrons are mainly stored in the exponential DOS of TiO<sub>2</sub>. Recombination should therefore be reduced with respect to classical TiO<sub>2</sub>

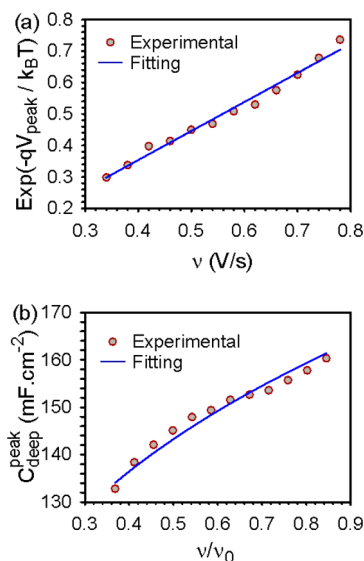


**Figure 4.** (a) Boltzmann type exponential factor calculated at the voltage of the deep trap capacitance peak versus scan rate. (b) Deep trap capacitance peak versus normalized scan rate. The red dots indicate the experimental data extracted from charge–discharge experiments, while the blue solid lines correspond to the fitting with the model developed in this Letter. The parameters used for the fitting are  $E_c = 0.4$  eV,<sup>34</sup>  $k_B T = 26$  meV, and  $L = 10$   $\mu$ m. Both plots were obtained from Figure 1c for the case of the submicrometer particles.

**Table 1. Extracted Parameters from Fitting of the Experimental Data of Figure 4**

parameters	submicrometer particles
$\alpha$	0.32
$N_L$	$8 \times 10^{18}$ cm <sup>-3</sup>
$N_t$	$2 \times 10^{16}$ cm <sup>-3</sup>
$\tau_0$	24 ms

nanoparticles where parasitic monoenergetic states can be observed. It should be pointed out that the contributions of  $g(E)$  and the monoenergetic surface state are dependent on sample composition, surface conditions, and even previous treatments. In fact, it is far from the scope of this Letter to discuss further the nature of these localized states.

In the determination of the chemical capacitance by IS, the nanostructured TiO<sub>2</sub> is at an equilibrium situation with respect to the given potential, and kinetic effects of traps are not usually observed.<sup>35</sup> Therefore, the peak observed in IS should correspond to the monoenergetic state. Indeed, measurements of IS for our samples, shown in Figure 5, indicate the presence of such a peak, and the determination of parameters for both DOS contributions is in good agreement with that of the multiple scan rate method developed above (see the SI for further explanations).

We shall now comment on the equilibrium trapping time,  $\tau_0$ , obtained in Table 1. Note that  $\tau_0$  is inversely proportional to the electron capture kinetics ( $\beta_n$ ), as indicated by eq 3.  $\tau_0$  is of particular importance in the observation of the contribution of deep traps. When  $\tau_0$  is on a small time scale, that is, when trapping/detrapping kinetics is fast, higher scan rates are required in order to leave a substantial part of trapped carriers off thermodynamic equilibrium and observe the deep trap capacitance peak in charge–discharge measurements. Large scan rates are not desirable though because nonlinear effects

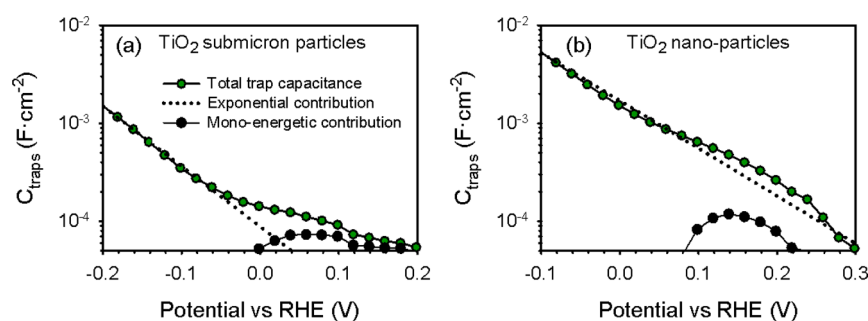


**Figure 5.** (a) Trap capacitance extracted from IS measurements for the case of the submicrometer particles (a) and the P25 particles (b). Both contributions to the total trap capacitance (the exponential and the monoenergetic capacitances) are also indicated.

may influence the measurements. Besides, for devices applications,  $\tau_0$  plays a critical role when the system, in steady state, is off equilibrium. For solar cells and solar fuel applications, the usual processes that break trap's equilibrium are illumination and charge transfer from the traps to another acceptor state. In the case of supra-band gap illumination, the electron trapping/detrapping kinetics must be compared to the one of the holes, which can be determined by IS.<sup>29,36</sup> In the case of charge transfer from the localized states to electrolyte species, the electron trapping kinetics must be compared to the charge-transfer rate<sup>37</sup> in order to understand the main recombination paths.

In summary, we have probed the kinetics and density of localized states of anatase TiO<sub>2</sub> submicrometer and P25 particles through chemical capacitance measurements by varying the scan rate of charge–discharge experiments. After establishing a general theoretical model for the localized states kinetics, we showed that it is possible to distinguish between two components of the DOS, that is, a monoenergetic level of deep traps and the deep traps of the exponential DOS of TiO<sub>2</sub>. Our results have shown that for both types of electrodes that we have studied, TiO<sub>2</sub> does display a peculiar capacitive peak that can be attributed to deep monoenergetic traps for the P25 particles as well as the deep traps of an exponential tail of localized states for the submicrometer particles. Those results constitute the first successful attempt to access the kinetics and density of localized states of nanocrystalline TiO<sub>2</sub> particles.

## ■ ASSOCIATED CONTENT

### ● Supporting Information

The TiO<sub>2</sub> preparation method, a HRSEM cross section of the P25 electrode, the detailed procedure for the extraction of the trap capacitance/voltage plots, the method of extraction of the shallow and deep trap capacitances, the method of extraction of the DOS parameters from the deep trap capacitance, a note on the role of the trapping kinetics for the observation of the deep trap capacitance, and a comparison between the trap capacitances measured by charge–discharge measurements and IS. This material is available free of charge via the Internet at <http://pubs.acs.org>.

## ■ AUTHOR INFORMATION

### Corresponding Author

\*E-mail: bisquert@uji.es.

### Notes

The authors declare no competing financial interest.

## ■ ACKNOWLEDGMENTS

The research leading to these results has received funding from the European Union Seventh Framework Program [FP7/2007–2013] under Grant Agreement 316494.

## ■ REFERENCES

- (1) Burschka, J.; Pellet, N.; Moon, S.-J.; Humphry-Baker, R.; Gao, P.; Nazeeruddin, M. K.; Grätzel, M. Sequential Deposition as a Route to High-Performance Perovskite-Sensitized Solar Cells. *Nature* **2013**, *499*, 316–320.
- (2) Leijtens, T.; Eperon, G. E.; Pathak, S.; Abate, A.; Lee, M. M.; Snaith, H. J. Overcoming Ultraviolet Light Instability of Sensitized TiO<sub>2</sub> with Meso-Superstructured Organometal Tri-Halide Perovskite Solar Cells. *Nat. Commun.* **2013**, *4*, 2885.
- (3) Kubacka, A.; Fernandez-Garcia, M.; Colon, G. Advanced Nanoarchitectures for Solar Photocatalytic Applications. *Chem. Rev.* **2012**, *112*, 1555–1614.
- (4) Fujishima, A.; Honda, K. Electrochemical Photolysis of Water at a Semiconductor Electrode. *Nature* **1972**, *238*, 37–38.
- (5) Armstrong, G.; Armstrong, A. R.; Bruce, P. G.; Reale, P.; Scrosati, B. TiO<sub>2</sub>(B) Nanowires as an Improved Anode Material for Lithium-Ion Batteries Containing LiFePO<sub>4</sub> or LiNi<sub>0.5</sub>Mn<sub>1.5</sub>O<sub>4</sub> Cathodes and a Polymer Electrolyte. *Adv. Mater.* **2006**, *18*, 2597–2600.
- (6) Schwarzburg, K.; Willig, F. Influence of Trap Filling on Photocurrent Transients in Polycrystalline TiO<sub>2</sub>. *Appl. Phys. Lett.* **1991**, *58*, 2520–2522.
- (7) Bisquert, J. Beyond the Quasi-Static Approximation: Impedance and Capacitance of an Exponential Distribution of Traps. *Phys. Rev. B* **2008**, *77*, 235203.
- (8) Bisquert, J.; Marcus, R. A. Device Modeling of Dye-Sensitized Solar Cells. *Top. Curr. Chem.* **2013**, DOI: 10.1007/1128\_2013\_1471.
- (9) Frese, K. W.; Morrison, S. R. Electrochemical Measurements of Interface States at the GaAs/Oxide Interface. *J. Electrochem. Soc.* **1979**, *126*, 1235–1241.
- (10) Hulea, I. N.; Brom, H. B.; Houtepen, A. J.; Vanmaekelbergh, D.; Kelly, J. J.; Meulenkaamp, E. A. Wide Energy-Window View on the Density of States and Hole Mobility in Poly(p-Phenylene Vinylene). *Phys. Rev. Lett.* **2004**, *93*, 166601.
- (11) Bisquert, J. Chemical Capacitance of Nanostructured Semiconductors: Its Origin and Significance for Heterogeneous Solar Cells. *Phys. Chem. Chem. Phys.* **2003**, *5*, 5360–5364.
- (12) Lee, P. A. Density of States and Screening near the Mobility Edge. *Phys. Rev. B* **1982**, *26*, 5882–5885.
- (13) Bisquert, J.; Fabregat-Santiago, F.; Mora-Seró, I.; Garcia-Belmonte, G.; Barea, E. M.; Palomares, E. A Review of Recent Results on Electrochemical Determination of the Density of Electronic States of Nanostructured Metal-Oxide Semiconductors and Organic Hole Conductors. *Inorg. Chim. Acta* **2008**, *361*, 684–698.
- (14) Berger, T.; Monllor-Satoca, D.; Jankulovska, M.; Lana-Villarreal, T.; Gómez, R. The Electrochemistry of Nanostructured Titanium Dioxide Electrodes. *ChemPhysChem* **2012**, *13*, 2824–2875.

- (15) Berger, T.; Anta, J. A.; Morales-Florez, V. Spectroscopic Properties of Electrochemically Populated Electronic States in Nanostructured TiO<sub>2</sub> Films: Anatase versus Rutile. *Phys. Chem. Chem. Phys.* **2013**, *15*, 13790–13795.
- (16) Henderson, M. A. A Surface Science Perspective on Photocatalysis. *Surf. Sci. Rep.* **2011**, *66*, 185–297.
- (17) Monroe, D.; Kastner, M. A. Exactly Exponential Band Tail in a Glassy Semiconductor. *Phys. Rev. B* **1986**, *33*, 8881–8884.
- (18) Schiff, E. A. Drift-Mobility Measurements and Mobility Edges in Disordered Silicons. *J. Phys.: Condens. Matter* **2004**, *16*, S5265.
- (19) Nunzi, F.; Mosconi, E.; Storchi, L.; Ronca, E.; Selloni, A.; Grätzel, M.; De Angelis, F. Inherent Electronic Trap States in TiO<sub>2</sub> Nanocrystals: Effect of Saturation and Sintering. *Energy Environ. Sci.* **2013**, *6*, 1221–1229.
- (20) Kavan, L.; Kratochvilova, K.; Grätzel, M. Study of Nanocrystalline TiO<sub>2</sub> (Anatase) Electrode in the Accumulation Regime. *J. Electroanal. Chem.* **1995**, *394*, 93–102.
- (21) de Jongh, P. E.; Vanmaekelbergh, D. Investigation of the Electronic Properties of Nanocrystalline Particulate TiO<sub>2</sub> Electrodes by Intensity-Modulated Photocurrent Spectroscopy. *J. Phys. Chem. B* **1997**, *101*, 2716–2722.
- (22) Boschloo, G.; Fitzmaurice, D. Spectroelectrochemical Investigation of Surface States in Nanostructured TiO<sub>2</sub> Electrodes. *J. Phys. Chem. B* **1999**, *103*, 2228–2231.
- (23) Wang, H.; He, J.; Boschloo, G.; Lindström, H.; Hagfeldt, A.; Lindquist, S. Electrochemical Investigation of Traps in a Nanostructured TiO<sub>2</sub> Film. *J. Phys. Chem. B* **2001**, *105*, 2529–2533.
- (24) Schwanitz, K.; Weiler, U.; Hunger, R.; Mayer, T.; Jaegermann, W. Synchrotron-Induced Photoelectron Spectroscopy of the Dye-Sensitized Nanocrystalline TiO<sub>2</sub>/Electrolyte Interface: Band Gap States and Their Interaction with Dye and Solvent Molecules. *J. Phys. Chem. C* **2006**, *111*, 849–854.
- (25) Yim, C. M.; Pang, C. L.; Thornton, G. Oxygen Vacancy Origin of the Surface Band-Gap State of TiO<sub>2</sub> (110). *Phys. Rev. Lett.* **2010**, *104*, 036806.
- (26) Scheiber, P.; Fidler, M.; Dulub, O.; Schmid, M.; Diebold, U.; Hou, W.; Aschauer, U.; Selloni, A. (Sub)Surface Mobility of Oxygen Vacancies at the TiO<sub>2</sub> Anatase (101) Surface. *Phys. Rev. Lett.* **2012**, *109*, 136103.
- (27) Zhang, J.; Hughes, T. F.; Steigerwald, M.; Brus, L.; Friesner, R. A. Realistic Cluster Modeling of Electron Transport and Trapping in Solvated TiO<sub>2</sub> Nanoparticles. *J. Am. Chem. Soc.* **2013**, *134*, 12028–12042.
- (28) Wang, H.; Lewis, J. P. Localization of Frontier Orbitals on Anatase Nanoparticles Impacts Water Adsorption. *J. Phys. Chem. C* **2009**, *113*, 16631–16637.
- (29) Bertoluzzi, L.; Bisquert, J. Equivalent Circuit of Electrons and Holes in Thin Semiconductor Films for Photoelectrochemical Water Splitting Applications. *J. Phys. Chem. Lett.* **2012**, *3*, 2517–2522.
- (30) Bisquert, J.; Zaban, A.; Salvador, P. Analysis of the Mechanisms of Electron Recombination in Nanoporous TiO<sub>2</sub> Dye-Sensitized Solar Cells. Nonequilibrium Steady-State Statistics and Interfacial Electron Transfer via Surface States. *J. Phys. Chem. B* **2002**, *106*, 8774–8782.
- (31) Orenstein, J.; Kastner, M. A. Thermalization and Recombination in Amorphous Semiconductors. *Solid State Commun.* **1981**, *40*, 85–89.
- (32) Bertoluzzi, L.; Badia-Bou, L.; Fabregat-Santiago, F.; Gimenez, S.; Bisquert, J. Interpretation of Cyclic Voltammetry Measurements of Thin Semiconductor Films for Solar Fuel Applications. *J. Phys. Chem. Lett.* **2013**, *4*, 1334–1339.
- (33) Gottesman, R.; Tirosh, S.; Barad, H.-N.; Zaban, A. Direct Imaging of the Recombination/Reduction Sites in Porous TiO<sub>2</sub> Electrodes. *J. Phys. Chem. Lett.* **2013**, *4*, 2822–2828.
- (34) Fujishima, A.; Rao, T. N.; Tryk, D. A. Titanium Dioxide Photocatalysis. *J. Photochem. Photobiol. C* **2000**, *1*, 1–21.
- (35) Bisquert, J.; Fabregat-Santiago, F.; Mora-Seró, I.; Garcia-Belmonte, G.; Barea, E. M.; Palomares, E. A Review of Recent Results on Electrochemical Determination of the Density of Electronic States of Nanostructured Metal-Oxide Semiconductors and Organic Hole Conductors. *Inorg. Chim. Acta* **2008**, *361*, 684–698.
- (36) Bertoluzzi, L.; Boix, P. P.; Mora-Sero, I.; Bisquert, J. Theory of Impedance Spectroscopy of Ambipolar Solar Cells with Trap-Mediated Recombination. *J. Phys. Chem. C* **2013**, DOI: 10.1021/jp411004e.
- (37) Bisquert, J. Theory of the Impedance of Charge Transfer via Surface States in Dye-Sensitized Solar Cells. *J. Electroanal. Chem.* **2010**, *646*, 43–51.